Log-validated FWI with wavelet phase and amplitude updating applied on Hussar data

Sergio Romahn and Kris Innanen

ABSTRACT

The estimation of the wavelet that is used for the forward modelling of synthetic shots is one of the main challenges that we must face when applying FWI on real data. We show in this report the negative effects of an incorrect wavelet and propose a methodology to mitigate this problem. We apply phase-shift plus interpolation (PSPI) migration with well calibration instead of reverse time migration (RTM) and line search to produce the velocity perturbation. The use of PSPI reduces the computational time, and we take advantage of this fact to implement our methodology. The process starts with an estimated wavelet that has similar frequency content than the seismic data. This wavelet does not have the optimal amplitude and phase for reproducing the observed shots. In order to address this problem, we migrate and stack the observed and modelled shots separately. Then we convert both datasets from depth to time by using the current velocity model. The comparison of these reflectivity datasets in time domain provides the elements for the estimation of an amplitude and phase that make the modelled data more similar to the observed data. Next, we take the difference between the observed and the amplitude-and-phase corrected modelled data to create the gradient. After that, we calibrate the gradient with well information to produce the velocity perturbation. The amplitude-and-phase correction estimated in this way is applied to update the wavelet that will be used in the next iteration. We applied this methodology on synthetic and Hussar datasets obtaining encouraging results.

INTRODUCTION

FWI is a procedure that extracts information from seismic data by fitting observed and synthetic shots generated by wavefield modelling. Lailly (1983) described the inversion as a sequence of prestack migrations of the residuals and provided the mathematical basis for FWI. Contemporary to Lailly, Tarantola (1984) arrived to a similar idea: he explained the solution of the inverse problem as an iterative methodology that consists of a forward propagation of the sources in the current model and backward propagation of the data residuals. The correlation between these two wavefields, which can be seen as the RTM of the data residual, leads to a correction of the model parameters. The idea of using any type of depth migration to produce the gradient was introduced by Margrave et al. (2010). The authors used PSPI migration and highlighted its suitability of selecting the frequencies that we want to use in each iteration. Examples of experiments based on the PSPI gradient are the works of Pan et al. (2014), Margrave (2014), Guarido et al. (2014), Arenrin and Margrave (2015), and Romahn and Innanen (2017). In order to obtain the velocity perturbation that will be used to update the model, Margrave et al. (2010) calibrated the PSPI gradient by matching it to the velocity residual (the difference between actual velocity and current velocity model) at the well. When well calibration is used instead of a line search to scale the gradient, the minimization of the data residuals is neglected and the inversion relies on the decrement of the error of the velocity model at the well location. Romahn and Innanen (2018) compared the performance of well calibration and line search and found that the

results are similar for the case of non complex geology. In the same report, the authors validated that the RTM gradient can be substituted by other migration method, for instance, PSPI. We retake the ideas of a PSPI gradient and well-log calibration in this work.

One problem that arises when we want to apply seismic inversion on real data is the unknown wavelet. Lee and Kim (2003) proposed an algorithm in which the source spectrum is eliminated by constructing a normalized wavefield in the Fourier domain, resulting in a source independent FWI. Liu et al. (2016) explored a similar idea in the time domain where the observed shots are convolved with a reference trace from the modelled wavefield and the modelled wavefield is convolved with a reference trace from the observed wavefield, in an attempt to remove the source wavelet. Synthetic examples show great potential in these ideas; however, problems such as slow converge and sensitivity to local mimima have prevented the successful application on real data.

We propose a methodology where the observed and modelled data are migrated and stacked separately and taken from depth to time domain by using the current velocity model (initial model for iteration one). Through the comparison of these two reflectivity datasets in time domain we are able to estimate an amplitude and phase that make the modelled data more similar to the observed data. The difference between observed and amplitude-and-phase updated modelled data produces a gradient that is calibrated with well-log information to obtain a velocity perturbation. The amplitude and phase correction are also applied to the wavelet that will be used in the next iteration. The results with synthetic data and Hussar dataset corroborate the feasibility of this methodology.

THEORY

Full waveform inversion with amplitude and phase updating

Standard FWI is a local optimization procedure. We start with an initial model and iteratively update it, so that after a number of iterations the model is able to produce synthetic data in reasonable agreement to the observed data. In our case, we are not focused in the minimization of the objective function because we don't use, for instance, line search to scale the gradient. When using well calibration, we focus on finding the velocity perturbation that makes our new velocity model more similar to the velocities measured in the well.

The basis of the inversion is given by equation 1 in what Margrave et al. (2010) called the fundamental theorem of FWI. This equation shows how the velocity update is obtained from a conveniently scaled gradient. The gradient of the objective function (equation 2) with respect to the model parameter is equivalent to the application of RTM to the data residuals in standard FWI.

$$\delta v(x,z) = \lambda \nabla_v \phi_k(x,z,w) = \lambda \int \sum_{s,r} \omega^2 \hat{\Psi}_s(x,z,\omega) \delta \hat{\Psi}^*_{r(s),k}(x,z,\omega) d\omega \qquad (1)$$

$$\phi_k = \sum_{s,r} (\Psi - \Psi_k)^2 \tag{2}$$

where $\delta v(x,z)$ is the velocity update, λ scales the gradient that in our case is done by applying well calibration, ∇_v is the gradient with respect to the velocity model v, $\phi_k(x,z,w)$ is the objective function, w is angular frequency, $\hat{\Psi}_s(x,z,\omega)$ is a model of the source wavefield for source s propagated to all (x,z), $\delta\hat{\Psi}^*_{r(s),k}(x,z,\omega)$ is the k^{th} data residual for source s back propagated to all (x,z), $*$ means complex conjugation. The residual $\delta\hat{\Psi}^*_{r(s),k}(x,z,\omega)$ is the difference between observed data Ψ_r and modeled data $\Psi_{r,k}$.

If we use PSPI migration instead of RTM and consider constant density, equation 1 can be expressed as:

$$\delta v(x,z) = \lambda Imp(\delta R) \tag{3}$$

where Imp denotes impedance inversion and δR is the pseudo reflectivity obtained by applying PSPI migration to the data residuals with a deconvolution imaging condition as shown in equation 4. We apply impedance inversion because PSPI migration produces reflectivity. In this way we can go from reflectivity to velocity units. The deconvolution imaging condition helps to compensate the spherical divergence of the wavefield (Margrave et al. (2010) and Pan et al. (2013)).

$$\delta R = \int \sum_{s,r} \frac{\delta U_r(x,z,\omega) D^*_s(x,z,\omega)}{D_s(x,z,\omega) D^*_s(x,z,\omega) + \mu I_{max}(z)} d\omega \tag{4}$$

where $\delta U_r(x,z,\omega)$ is the upgoing receiver data residual wavefield, $D_s(x,z,\omega)$ is the downgoing source wavefield, μ is a small non-negative stability constant, and $I_{max}(z) = max[D_s(x,z,\omega)D^*_s(x,z,\omega)]$.

In equation 5 we separated the upgoing data residual wavefield δU_r into two wavefields, one for the observed data (U_o) and another one for the modelled data (U_m):

$$\delta U_r(x,z,\omega) = U_o(x,z,\omega) - U_m(x,z,\omega) \tag{5}$$

In this way we produce the observed and modelled reflectivity ($R_{o,z}$ and $R_{m,z}$) in depth separately as shown by equations 6 and 7:

$$R_{o,z} = \int \sum_{s,r} \frac{U_o(x,z,\omega) D^*_s(x,z,\omega)}{D_s(x,z,\omega) D^*_s(x,z,\omega) + \mu I_{max}(z)} d\omega \tag{6}$$

$$R_{m,z} = \int \sum_{s,r} \frac{U_m(x,z,\omega) D_s^*(x,z,\omega)}{D_s(x,z,\omega) D_s^*(x,z,\omega) + \mu I_{max}(z)} d\omega \tag{7}$$

It's at this point where we have the opportunity to mitigate the effect of a wrong initial wavelet.

The next step consists on converting both $R_{o,z}$ and $R_{m,z}$ from depth to time by using the model of the current iteration. The reflectivity in time $R_{o,t}$ and $R_{m,t}$ are used to obtain the cost function in equation 8:

$$\epsilon_R = \sum (R_{o,t} - R_{m,t})^2 \tag{8}$$

After that we search for an amplitude A and a phase ϕ that reduce the value of ϵ_R. These amplitude and phase then are used to correct $R_{m,t}$. If we are not able to find an amplitude and phase that minimize equation 8, then $R_{m,t}$ is not modified.

The wavelet is only updated if the estimated amplitude and phase minimize the data residuals. If this condition is not met, we continue with the same wavelet. We repeat the frequency range when the wavelet is updated in order to maximize the extraction of information in this frequency band.

Next, we obtain a pseudo gradient of reflectivity by applying the difference between $R_{o,t}$ and the amplitude-and-phase updated $R_{m,t}(A, \phi)$:

$$\delta R_t = R_{o,t} - R_{m,t}(A, \phi) \tag{9}$$

The final gradient is produced when we apply impedance inversion to δR:

$$g = Imp(\delta R) \tag{10}$$

Finally, we calibrate the gradient with well-log information of the model parameter in order to produce the velocity perturbation. The process consists in comparing the gradient trace at the well location to the velocity residual at the well. From this comparison, we are able to estimate the amplitude scalar and phase rotation that make the gradient trace more like the velocity residual. The scalar and phase rotation are found such that the difference between the gradient trace and the velocity residual is minimized by least squares. A convolution matched filter λ, obtained with this amplitude and phase, is applied to the whole gradient to obtain the velocity perturbation.

The flow chart of the process described above is shown in Figure 1. In the next section, we show the implementation of this methodology on synthetic data.

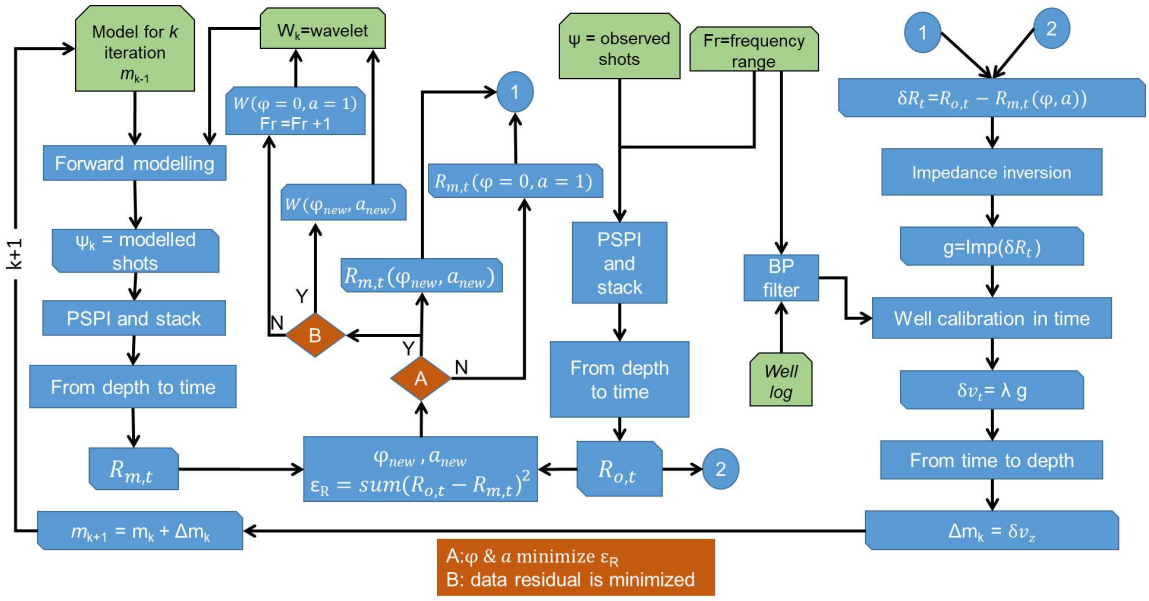

FIG. 1. FWI flow with well-log calibration and amplitude-and-phase updating.

NUMERICAL EXAMPLES

The model used for the synthetic example is characterized by a shallow anticline that constitutes a low velocity reservoir trap surrounded by a relatively high velocity medium (Figure 2A). There is also a low velocity stratigraphic trap located at a depth of 800 m at the left-hand side of the model. A shallow high velocity body at a depth of 300 m is located at the right-hand side of the model. The shots, which will be considered the observed data, were generated by applying constant-density acoustic finite-difference modelling through the velocity model. We used a minimum-phase wavelet rotated by 60 degrees with a dominant frequency of 10 Hz as a seismic source. The source and receiver intervals are 120 and 10 meters, respectively. The total number of shots is 83. The initial model for the inversion was generated by applying a Gaussian smoother with a half-width of 200 m to the true model (Figure 2B). An example of a shot located at the middle of the model is shown in Figure 2C. The initial frequency range was from 1 to 6 Hz, then it was moved up by 1 Hz in each iteration. The calibration well C is located at the middle of the model, its top and base are 400 and 900 m, respectively.

Impact of a wrong wavelet in the inversion

In the first example we wanted to see the effect of a wrong wavelet in the inversion result without any amplitude-and-phase correction. In order to do so, we obtained an initial wrong wavelet by multiplying the true wavelet by 0.2 and rotating its phase by 90 degrees. The comparison between true and initial wavelets is shown in Figure 3. In this case the amplitude spectrum of both wavelets is exactly the same.

Figure 4 shows the negative impact in the inversion when we use the wrong wavelet displayed on Figure 3. The errors in the model, blind well B and calibration well C, tend

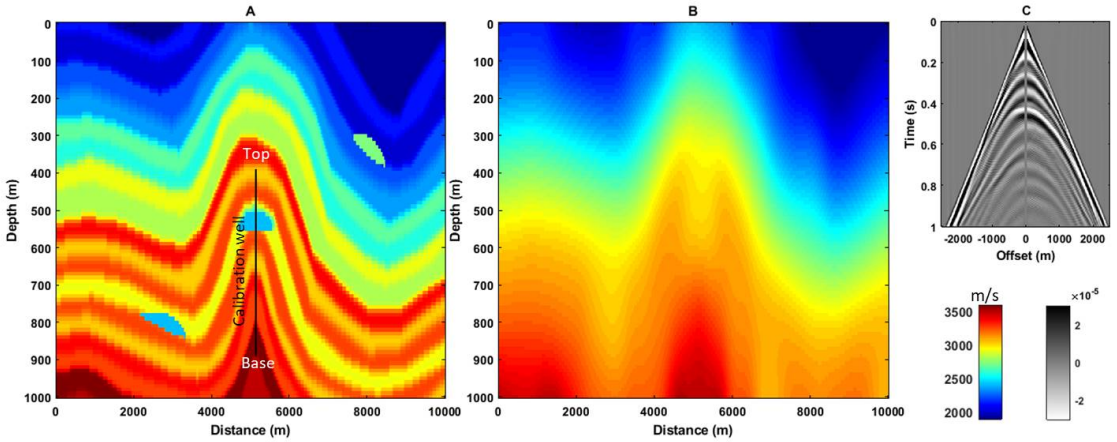

FIG. 2. A) True velocity model. The calibration well is located at the middle of the model and covers a depth interval from 400 to 900 m. B) Initial model. C) Observed shot located at the middle of the model.

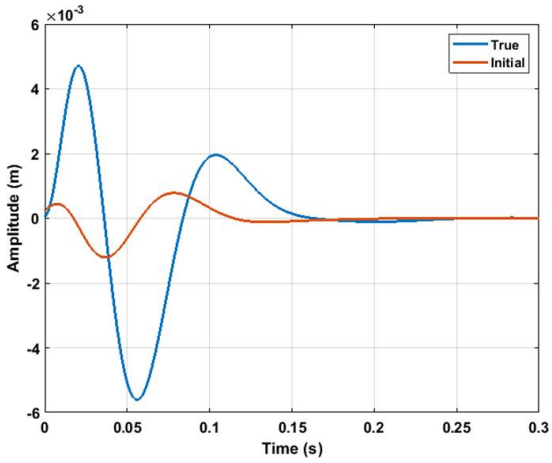

FIG. 3. The initial wavelet was obtained by multiplying the true wavelet by 0.2 and rotating its phase by 90 degrees.

to be greater in each iteration. A strong source footprint dominates the shallow zone and the velocities tend to be over or underestimated across the model. The fact that we were able to recover the main features of the model may be attributable to the well calibration process where the phase and amplitude of the gradient are modified to match the velocity residual at the well.

Applying amplitude-and-phase updating

For the next example we estimated an initial wavelet from the seismic data by using "waveletestimator" from CREWES-MATLAB tool box (Figure 5). The comparison of the estimated wavelet from the seismic and the true wavelet is shown in Figure 6. We observe that the amplitude and phase are totally different and their amplitude spectra partially match.

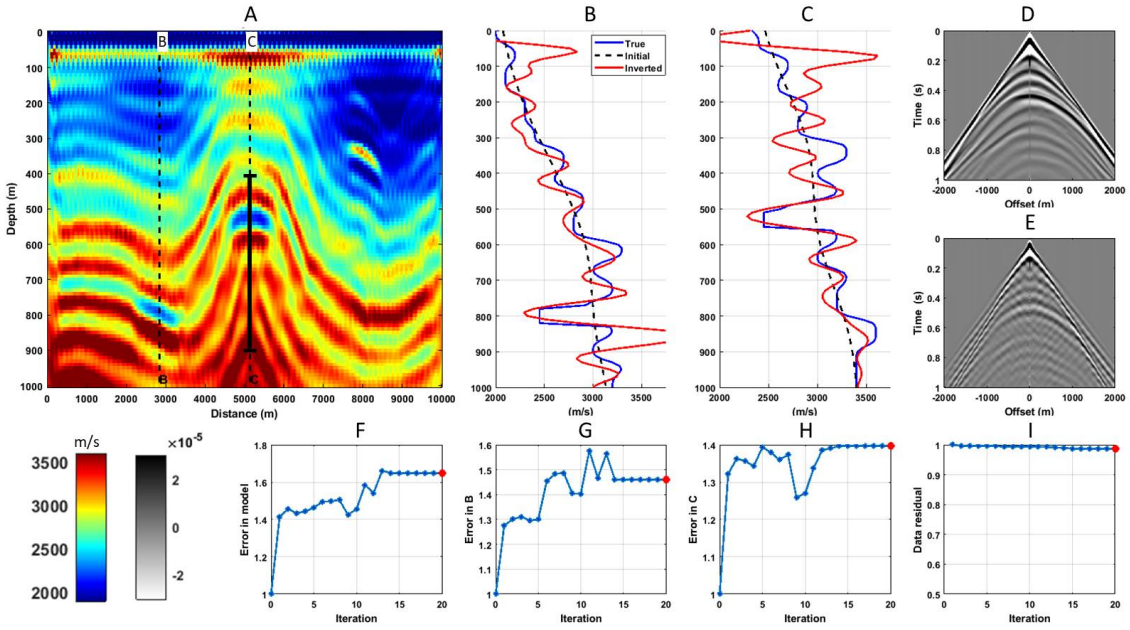

FIG. 4. A) Inverted model with the wrong initial wavelet of Figure 3 without applying any amplitude and phase correction. B) Inverted velocity in blind well B. C) Inverted velocity in calibration well C. D) Observed shot. E) Modelled shot. F) Error in inverted model. G) Error in blind well B. H) Error in calibration well C. I) L2N of data residuals.

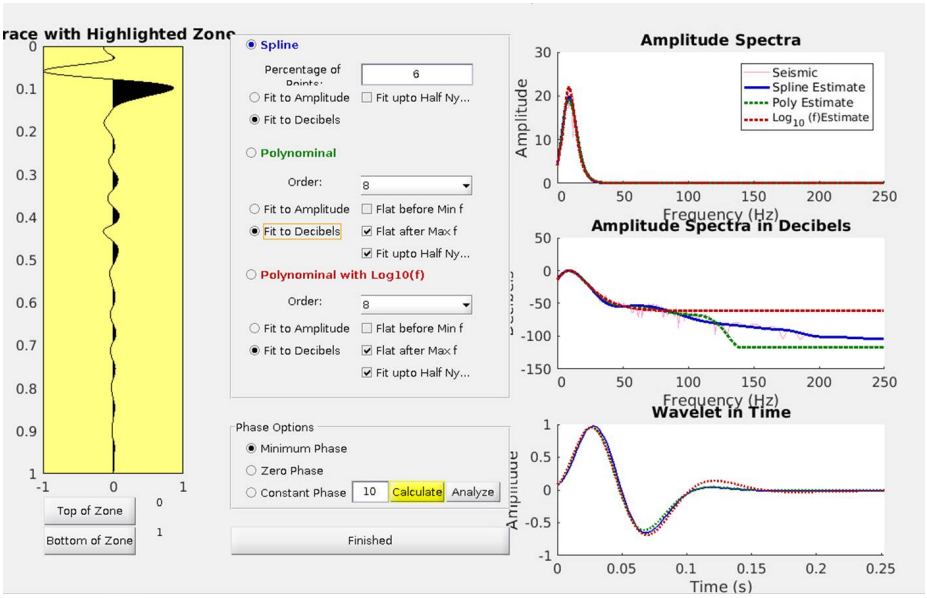

FIG. 5. Main screen of "waveletestimator" program. The options Spline of 6 points and fit to Decibel were chosen to estimate the minimum phase wavelet from the seismic data.

We applied our methodology to invert data with amplitude and phase updating and the result is shown in Figure 7. Here we are able to recover the true model diminishing most of the negative effect that the wrong wavelet produced in the previous example. The errors tend dramatically decrease after iteration 10 when the wavelet has been already corrected

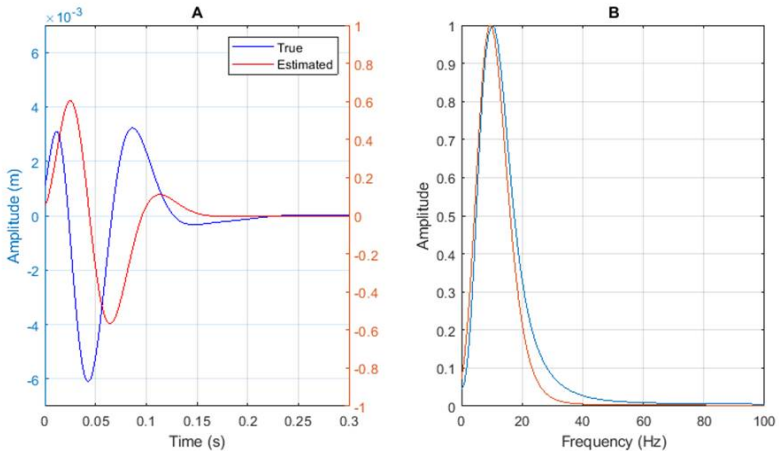

FIG. 6. A) Comparison of the true wavelet to the one estimated from the seismic data. B) Amplitude spectrum of the true wavelet in blue and estimated wavelet in red.

as it's shown in Figure 8. The amplitude and phase updates at each iteration are shown in Figure 9. We observe that the wavelet (blue curve) only changes for few iterations where the condition of decreasing the data residuals is met. On the other hand, the modelled reflectivity (in red) is subject to small amplitude and phase updates as we continue iterating.

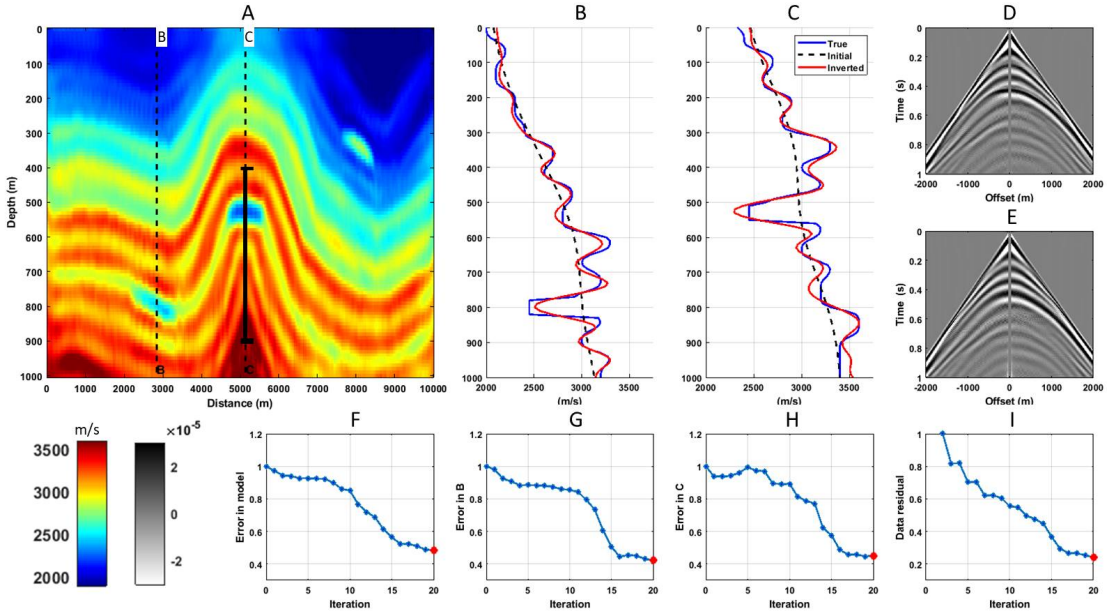

FIG. 7. A) Inverted model with the wrong initial wavelet estimated from the seismic data and applying the process of phase-and amplitude updating. B) Inverted velocity in blind well B. C) Inverted velocity in calibration well C. D) Observed shot. E) Modelled shot. F) Error in inverted model. G) Error in blind well B. H) Error in calibration well C. I) L2N of data residuals.

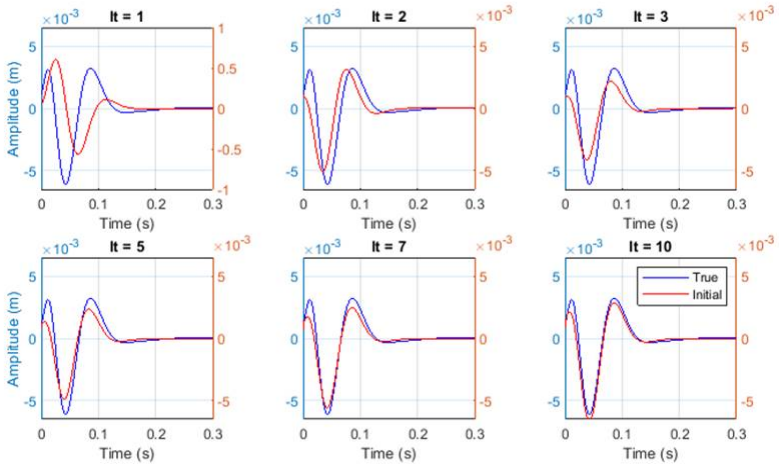

FIG. 8. Updated wavelet for selected iterations. The wavelet practically doesn't change after iteration 10.

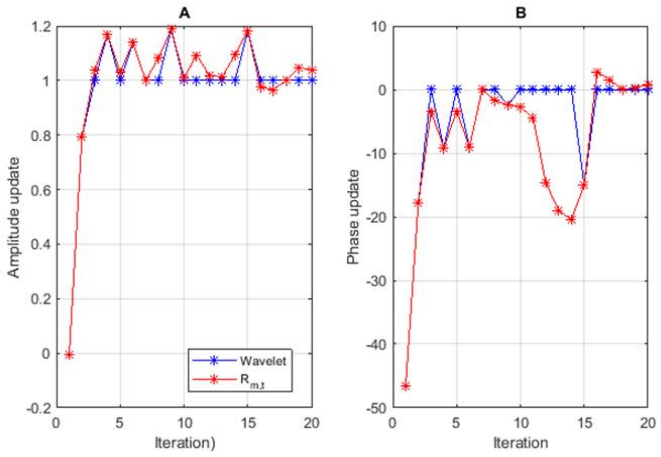

FIG. 9. A) Amplitude updates for the wavelet in blue and for the modelled reflectivity in red. B) Phase updates for the wavelet in blue and for the modelled reflectivity in red.

Effect of random noise

We added random noise in order to observe the effect of this factor in the amplitude-and-phase updating process. The inversion result is displayed in Figure 10. The presence of noise affects the continuity of the velocity layers in the final inverted model; however, the evolution of the updated wavelet in the first iterations (shown in Figure 11), is very similar than in the previous case where no noise is involved. This example shows that we are still able to recover information about the amplitude and phase of the true wavelet in the presence of random noise. The amplitude and phase updates at each iteration are shown in Figure 12. The wavelet only changes in few iterations, while the migrated modelled data still has important corrections before iteration 16.

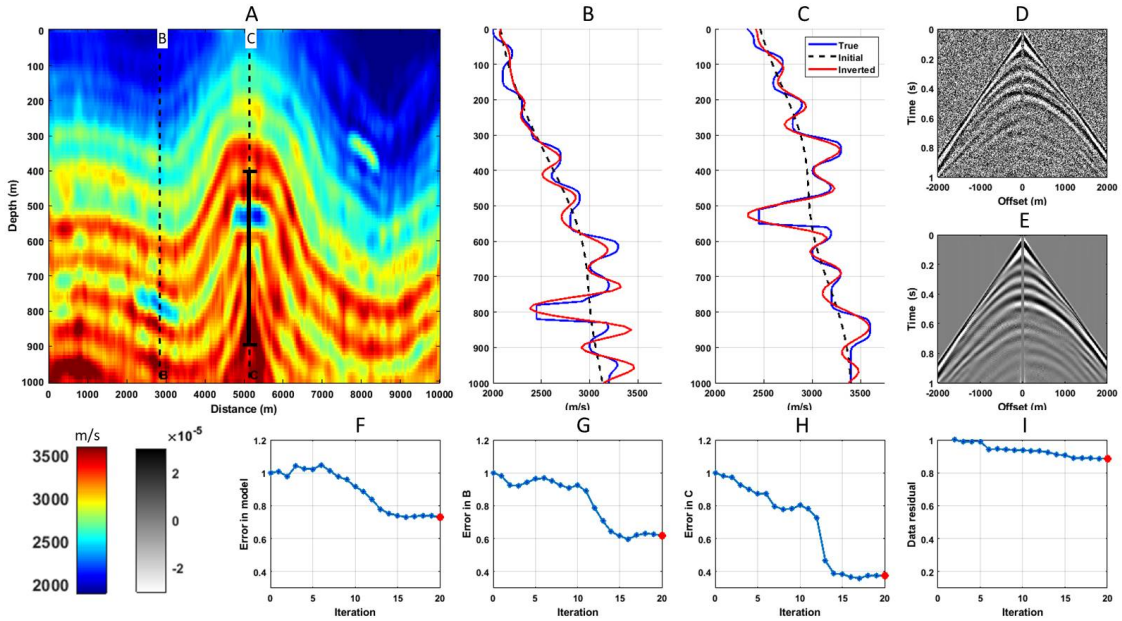

FIG. 10. A) Inversion model with an initial wavelet estimated from the seismic. We added random noise to make the experiment more realistic. We applied the process of phase-and amplitude updating. B) Inverted velocity in blind well B. C) Inverted velocity in calibration well C. D) Observed shot with noise. E) Modelled shot. F) Error in inverted model. G) Error in blind well B. H) Error in calibration well C. I) L2N of data residuals.

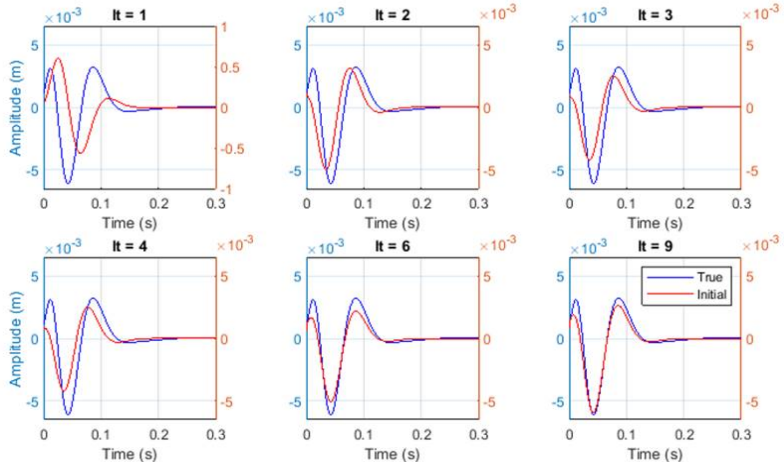

FIG. 11. Evolution of the inverted wavelet in the presence of noise for selected iterations .

APPLICATION ON HUSSAR DATA

The FWI methodology developed in this study was applied on Hussar 2D dataset. These data consist of 257 source stations spaced every 20 m approximately and 448 receiver stations spaced every 10 m, for a total length of 4.47 Km. Although originally acquired with a variety of sources and receivers (Margrave et al., 2011a), in this study we only use the vertical component of the accelerometer data recorded using 2 kg dynamite sources at 15 m depth. All receivers were live at every source point producing source gathers with

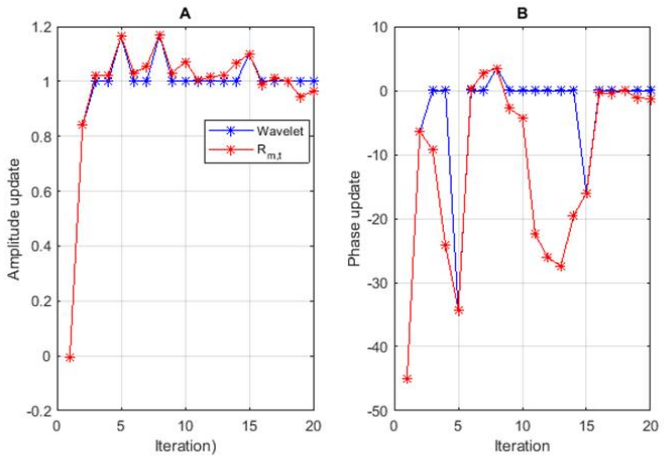

FIG. 12. A) Amplitude updates for the wavelet in blue and for the modelled reflectivity in red. B) Phase updates for the wavelet in blue and for the modelled reflectivity in red. Observed shots have random noise.

448 traces. Figure 13 shows the source and receiver distribution in the area and the location of the wells near Hussar survay.

The shots used in this work were processed by Isaac and Margrave (2011) and included radial filtering (Henley, 1999) to attenuate high-amplitude low-frequency source-generated noise and Gabor deconvolution (Margrave et al., 2011b) that corrects for the effects of source wavelet and anelastic attenuation. The data was processed to a final datum of 985 m. Examples of the processed shots are shown in Figure 14. We also applied a low-pass filter with a cutoff of 65 Hz and FK filtering to deal with the remnant linear source noise (Figure 15). The stack of the conditioned shots that were used for the inversion is shown in Figure 16. We only used a third of the shots and a maximum time of 1.32 seconds for the inversion. We mute the direct arrival in both observed and modelled shots

Well 14-34 was used to generate the initial model shown in Figure 17A and to calibrate the gradient in the inversion process. Wells 01-34 and 14-27 were used to verify the result.

Figure 18A shows the initial minimum-phase wavelet that was estimated from the seismic data by using "waveletestimator" from CREWES-MATLAB tool box. The dominant frequency is around 20 Hz as shown in the amplitude spectrum in Figure 18B.

Inversion result

Figure 19 shows the inversion result for Hussar dataset. At the zone, where we have significant seismic events from 0.8 seconds (approximately 1000 m of depth), the inverted velocity shows a reasonable agreement with the velocity measure in the wells. However, in the shallow zone where the lack of seismic information is evident, the inversion does not effectively perform. We can say that result is encouraging considering the difficulty of inverting onshore seismic data.

A final word about well 01-34: we found that the best match of the inverted velocity

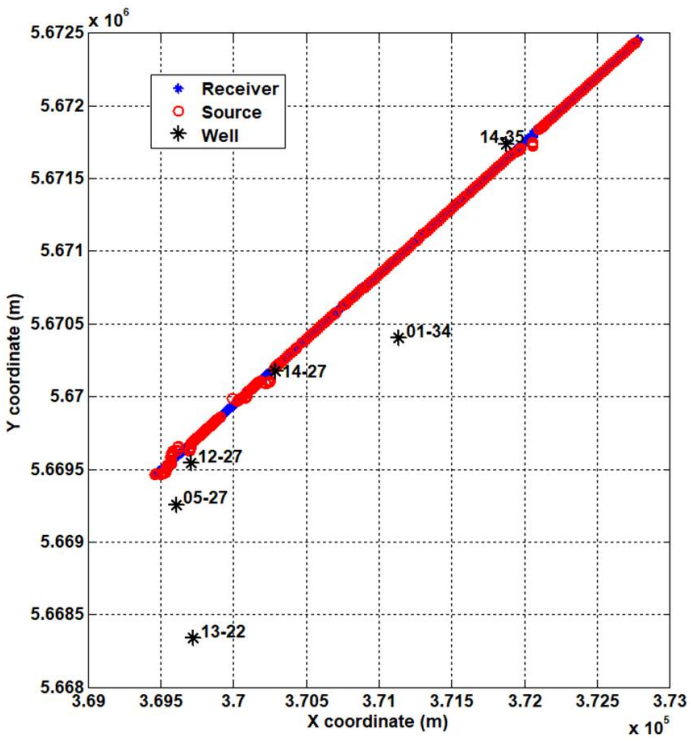

FIG. 13. Hussar survey. Source and receiver distribution and location of the wells near this 2D line.

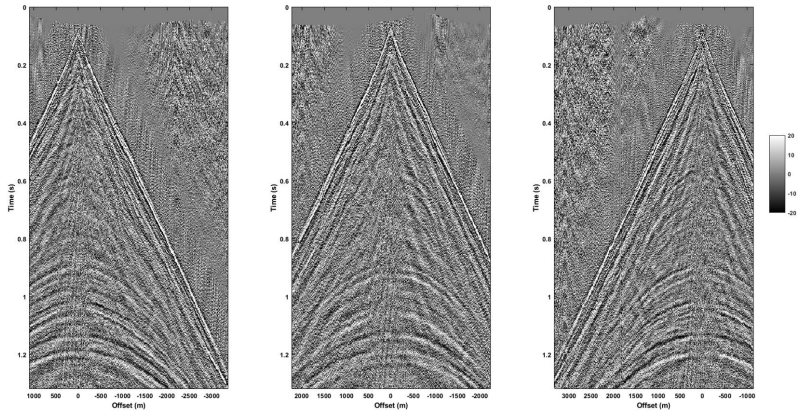

FIG. 14. Example of Hussar's shots used in the inversion. Radial filtering and Gabor deconvolution were applied.

and the log of well 01-34 was obtained where we moved the log 50 meters up. This well is 450 meters away of the seismic line, which suggests that the layers are dipping down to that direction about 6 degrees.

Figure 20 shows an observed and a modelled shots after 30 iterations and the L2N of the data residuals. The fact that the wavelet may potentially change in each iteration makes the data residuals unstable.

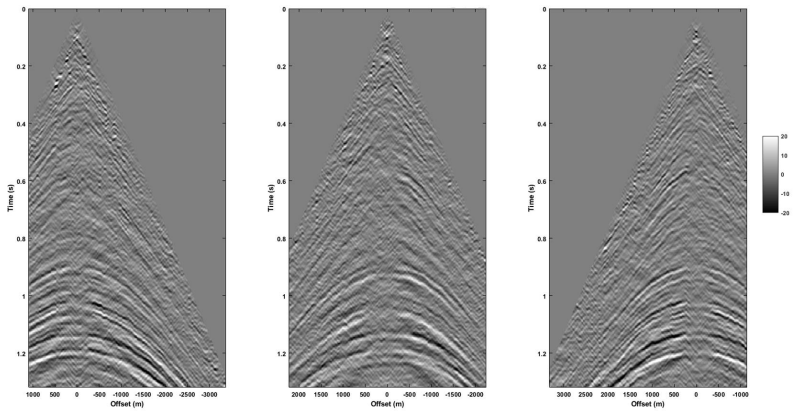

FIG. 15. We applied a low-pass filter with a cutoff of 65 Hz and FK filtering to obtain the final shots that were used in the inversion.

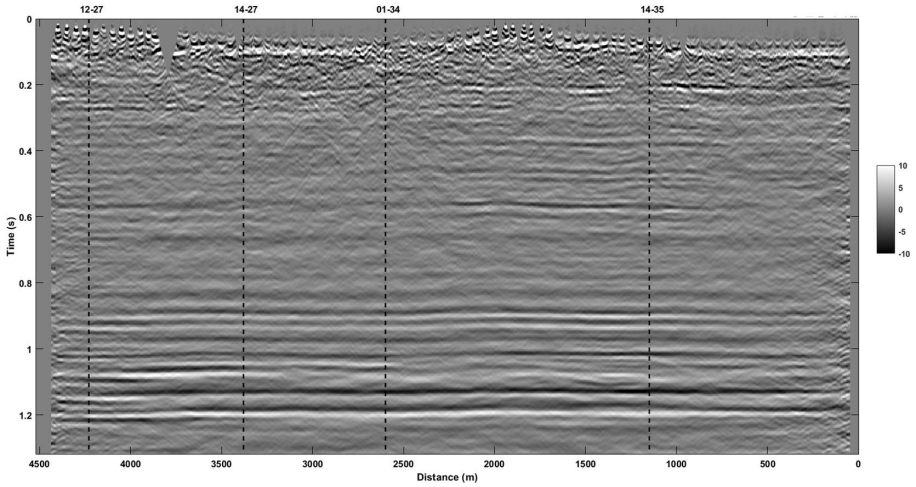

FIG. 16. Stack of shots after low-pass and FK filtering.

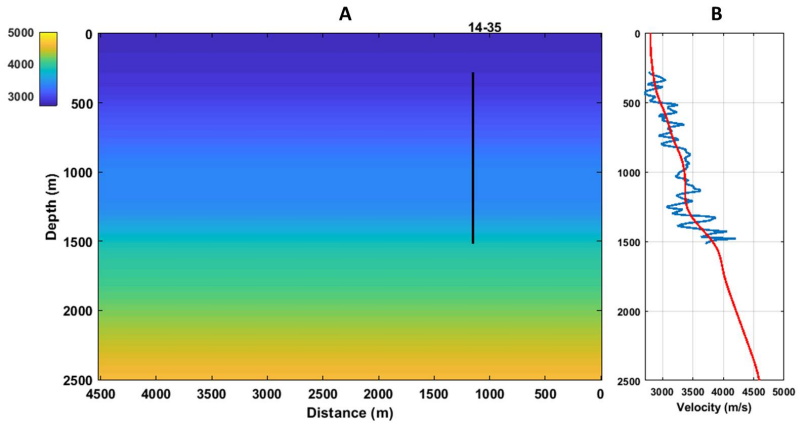

FIG. 17. A) Initial model for Hussar inversion. B) P-wave velocity in well 14-35 used to generate the initial model.

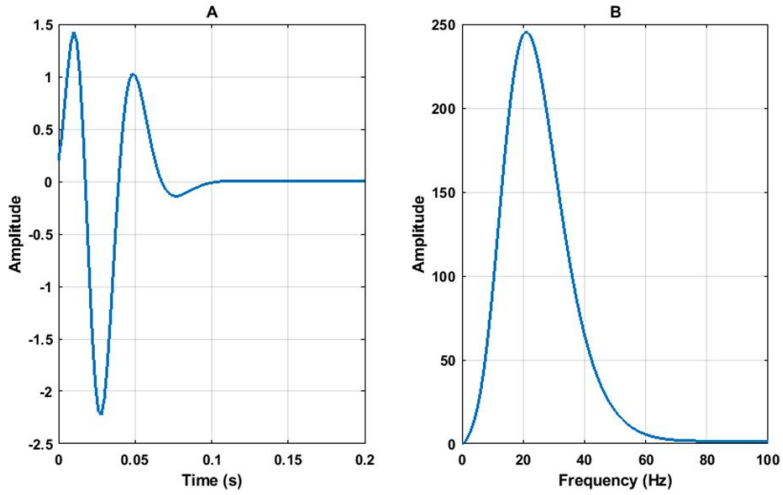

FIG. 18. A) Initial wavelet estimated from the seismic data. B) Amplitude spectrum.

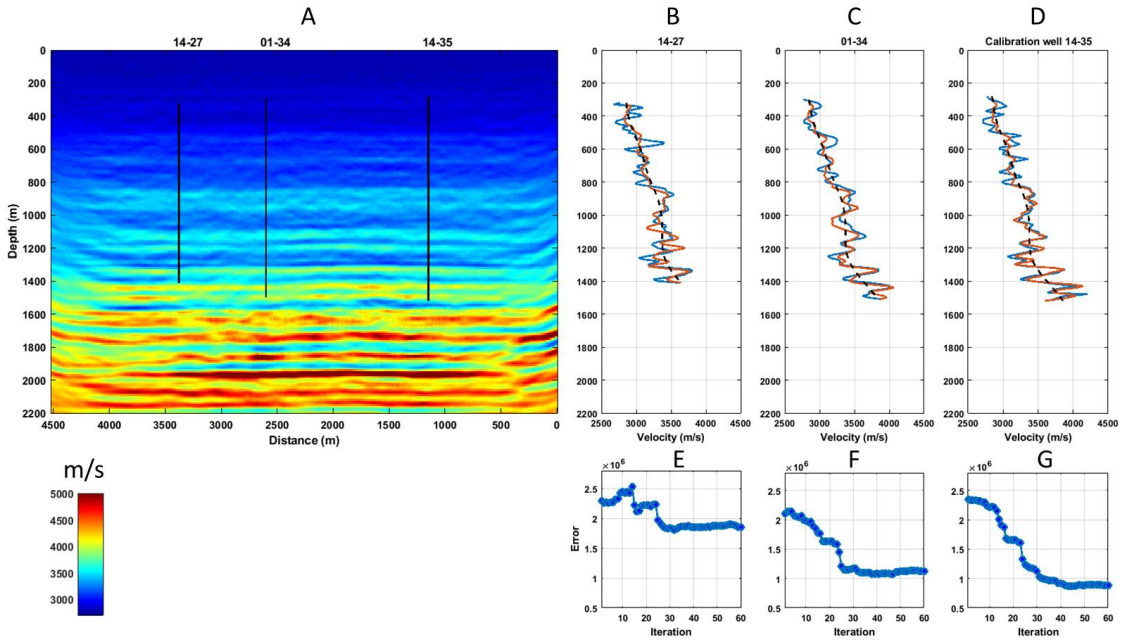

FIG. 19. A) Inverted model for Hussar dataset. B) Inverted velocity in well 14-27. C) Inverted velocity in well 01-34. D) Inverted velocity in calibration well 14-35. E) Error in inverted velocity for well 14-27. F) Error in inverted velocity for well 01-34. G) Error in inverted velocity for calibration well 14-35.

DISCUSSION

In the synthetic examples we saw that the amplitude-and-phase wavelet updates don't have significant changes after the first few iterations, showing stability in the process. This is not happening for the case of Hussar dataset as it's shown in Figures 21 and 22, where the evolution of the wavelet with iterations and the amplitude-and-phase updates are displayed. We observed that the updates of the wavelet are applied for certain iterations where

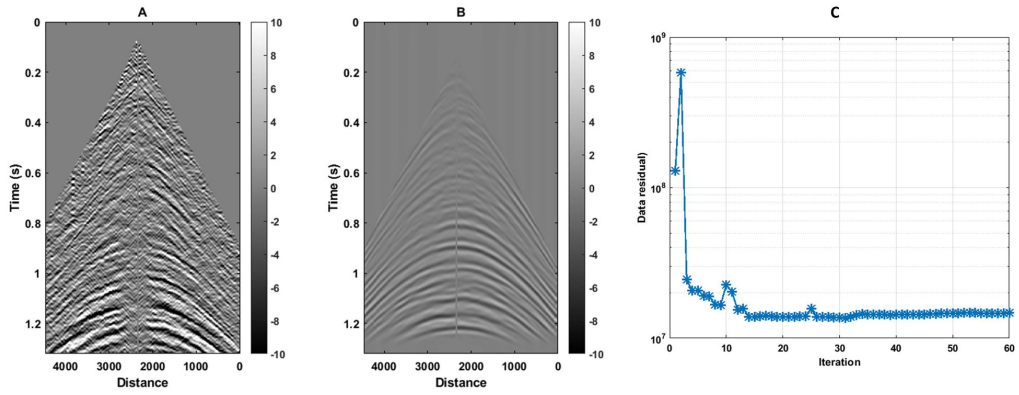

FIG. 20. A) Observed shot. B) Modelled shot after 30 iterations. C) L2N of the data residuals.

the condition of reducing the data residual is met, while the amplitude-and-phase updates for the modelled reflectivity are never stabilized. The latter suggests that the process of updating the modelled reflectivity before constructing the gradient has the greatest weight. This methodology seems to be robust enough to be applied on real data; however, there is still much to do in order to find the optimum wavelet.

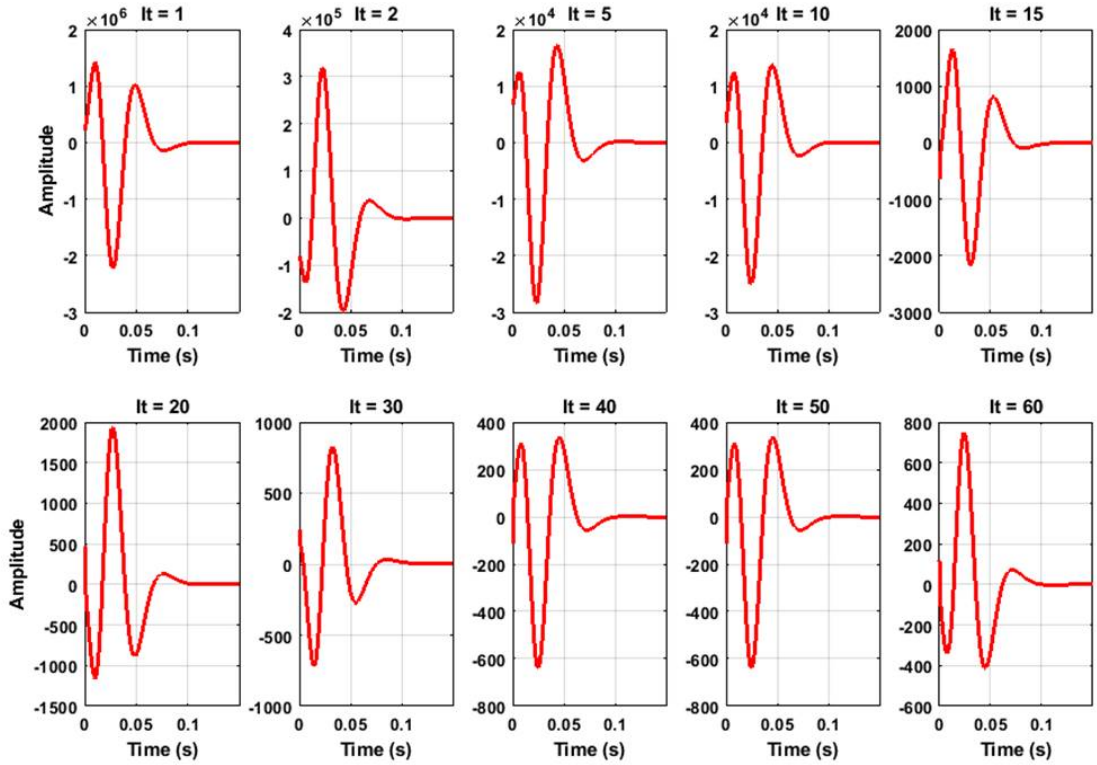

FIG. 21. Updated wavelet for selected iterations for Hussar dataset.

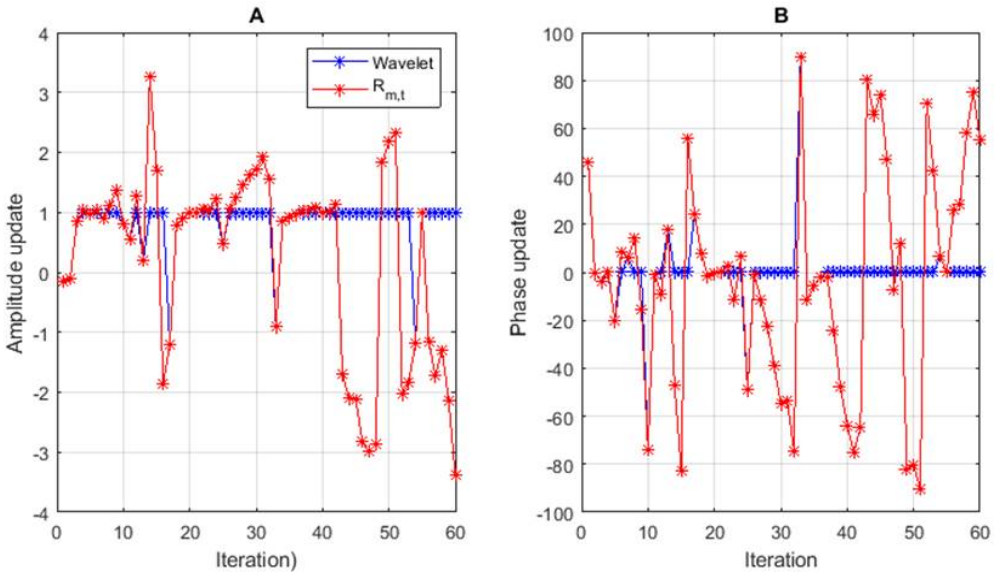

FIG. 22. A) Amplitude updates for the wavelet in blue and for the modelled reflectivity in red. B) Phase updates for the wavelet in blue and for the modelled reflectivity in red.

CONCLUSIONS

We proposed a methodology to diminish the negative impact that a wrong initial wavelet produces in the FWI process. Our methodology consists in separating the migration and stack of the observed and modelled data previous to the construction of the gradient. Experiments with synthetic data shows that when we compare these two datasets there is meaningful information that provides the elements to estimate an amplitude-and-phase correction in time domain. We applied this scheme to the Hussar dataset, obtaining encouraging results. However, the high variability of the wavelet for the case of real data, brings certain questions about the validity of the updated wavelet and suggests that the inversion relies on the matching process of the observed and modelled reflectivity datasets. In future work, we will address the issue of the instability of the updated wavelet that we saw in the real seismic data.

ACKNOWLEDGEMENTS

We thank the sponsors of CREWES. We acknowledge support from NSERC through the grant CRDPJ 461179-13. Author 1 thanks PEMEX and the government of Mexico for founding his research.

REFERENCES

Arenrin, B., and Margrave, G. F., 2015, Full waveform inversion of hussar synthetics: CREWES Research Report, **27**.

Guarido, M., Lines, L., and Ferguson, R., 2014, Full waveform inversion - a synthetic test using the pspi migration: CREWES Research Report, **26**.

Henley, D. C., 1999, Coherent noise attenuation in the radial trace domain: Introduction and demonstrationl: CREWES Research Report, **11**.

Isaac, J. H., and Margrave, G. F., 2011, Hurrah for hussar! comparisons of stacked datal: CREWES Research Report, **23**.

Lailly, P., 1983, The seismic inverse problem as a sequence of before stack migration: SIAM, 206–220.

Lee, K. H., and Kim, H. J., 2003, Source-independent full-waveform inversion of seismic data: Geophysics, **68**, No. 6, 2010–2015.

Liu, S., Meng, X., and Fu, L., 2016, Source wavelet independent time-domain full waveform inversion (fwi) of cross-hole radar data, *in* Geoscience and Remote Sensing Symposium (IGARSS), 2016 IEEE International, IEEE, 7485–7488.

Margrave, G. F., 2014, Post-stack iterative modeling migration and inversion (immi): CREWES Research Report, **27**.

Margrave, G. F., Bertram, M. B., Lawton, D. C., Innanen, K. A., Hall, K. W., Mewhort, L., and Hall, M., 2011a, The hussar low-frequency experimentl: CREWES Research Report, **23**.

Margrave, G. F., Fergurson, R. J., and Hogan, C. M., 2010, Full-waveform inversion with wave equation migration and well control: CREWES Research Report, **22**.

Margrave, G. F., Lamoureux, M. P., and Henley, D. C., 2011b, Gabor deconvolution: Estimating reflectivity by nonstationary deconvolution of seismic data: Geophysics, **76**, No. 3, W15–W30.

Pan, W., Margrave, G., and Innanen, K. A., 2013, On the role of the deconvolution imaging condition in full waveform inversion: CREWES Research Report, **25**.

Pan, W., Margrave, G. F., and Innanen, K. A., 2014, Iterative modeling migration and inversion (immi): Combining full waveform inversion with standard inversion methodology: 84th Ann. Internat. Mtg., SEG, Expanded Abastracts, 938–943.

Romahn, S., and Innanen, K. A., 2017, Iterative modeling, migration, and inversion: Evaluating the well-calibration technique to scale the gradient in the ful waveform inversion process: SEG Technical Program Expanded Abstracts 2017, 1583–1587.

Romahn, S., and Innanen, K. A., 2018, Fwi with wave equation migration: well validation vs data validation vs well-and-data validation: CREWES Research Report, **30**.

Tarantola, A., 1984, Inversion of seismic reflection data in the acoustic approximation: Geophysics, **49**, 1259–1266.